X-ray spectroscopy uncovering the effects of Cu based nanoparticle concentration and structure on Phaseolus vulgaris germination and seedling development.

Duran, N.M.; Savassa, S.M.; Lima, R.; De Almeida, R.; Linhares, F.; van Gestel, C.A.M.; Pereira de Carvalho, H.W.

published in
Journal of Agricultural and Food Chemistry
2017

DOI (link to publisher)
10.1021/acs.jafc.7b03014

document version
Publisher's PDF, also known as Version of record

JOURNAL OF AGRICULTURAL AND FOOD CHEMISTRY

Article

pubs.acs.org/JAFC

X-ray Spectroscopy Uncovering the Effects of Cu Based Nanoparticle Concentration and Structure on *Phaseolus vulgaris* Germination and Seedling Development

Nádia M. Duran,[†] Susilaine M. Savassa,[†] Rafael Giovanini de Lima,[†] Eduardo de Almeida,[†] Francisco S. Linhares,[‡] Cornelis A. M. van Gestel,[§] and Hudson W. Pereira de Carvalho*[,†]

[†]Laboratory of Nuclear Instrumentation (LIN), Center of Nuclear Energy in Agriculture (CENA), University of São Paulo (USP), Piracicaba, São Paulo 13416000, Brazil

[‡]Laboratory of Plant Development and Structure (LaBDEV), Center of Nuclear Energy in Agriculture (CENA), University of São Paulo (USP), Piracicaba, São Paulo 13416-000, Brazil

[§]Department of Ecological Science, Faculty of Science, Vrije Universiteit, De Boelelaan 1085, 1081HV Amsterdam, The Netherlands

Supporting Information

ABSTRACT: Nanoparticles properties such as solubility, tunable surface charges, and singular reactivity might be explored to improve the performance of fertilizers. Nevertheless, these unique properties may also bring risks to the environment since the fate of nanoparticles is poorly understood. This study investigated the impact of a range of CuO nanoparticles sizes and concentrations on the germination and seedling development of *Phaseolus vulgaris* L. Nanoparticles did not affect seed germination, but seedling weight gain was promoted by 100 mg Cu L^{-1} and inhibited by 1 000 mg Cu L^{-1} of 25 nm CuO and $CuSO_4$. Most of the Cu taken up remained in the seed coat with Cu hotspots in the hilum. X-ray absorption spectroscopy unraveled that most of the Cu remained in its pristine form. The higher surface reactivity of the 25 nm CuO nanoparticles might be responsible for its deleterious effects. The present study therefore highlights the importance of the nanoparticle structure for its physiological impacts.

KEYWORDS: *Phaseolus vulgaris, CuO nanoparticle, germination, X-ray based spectroscopy*

INTRODUCTION

In the past few years, a wide range of engineered nanoparticles, with unique physicochemical properties, has been launched on the market and consequently to the environment. Such properties make these materials suitable for applications that substantially differ from those of the usual bulk form. The nanoscale particle size of these materials increases the surface to volume ratio, thus an important fraction of the atoms lies on the surface. These surface atoms have different properties that those in bulk, thus affecting their solubility, light scattering and absorbance, conductivity, melting point, and catalytic properties.[1] Being present also in many daily life goods, nanoparticles can easily be released into the environment and reach the entire food chain. This possibility, which may result in toxicological effects on consumers,[2] remains so far uncertain and has been a matter of intense debate in recent years.

The development of nanotechnologies tailored for agricultural purposes can result in a more rational use of pesticides, biocides, and fertilizers,[3,4] potentially reducing the usage of these hazardous products in agricultural practices. Such innovations could lead to cost reduction, less nutrient leaching, and preservation of the desirable soil microbiota. In this context, we highlight the possibility of employing nanotechnology for seed coating.[5] Seed coating is an attractive way for micronutrient delivery. It has the potential to improve seedling growth and crop productivity[6] while treated seeds generally germinate faster and more synchronized than nontreated seeds.[7] Compared to soil fertilization, seed treatment is an easier and cost-effective way requiring a lower quantity of nutrients.[6] A significant yield increase was observed when wheat seeds were treated with a low dose of Cu-EDTA (0.04 kg ha^{-1}).[8]

The uptake of nanoparticles by plants occurs not only through the root system[9] but also via leaves[10] and seeds.[11] Studies regarding the effects of the interaction between nanoparticles and plants are not consensual. While some studies show that nano ZnO promoted root elongation in peanut[12] and soybean,[13] others showed similar results of nano CeO_2 treatments on coriander,[14] corn, and cucumber,[15] while studies on tobacco[16] and basil[17] showed detrimental effects on germination and growth upon exposure to nano TiO_2.

The effects of nanoparticle exposure do not only vary with the plant species, they also depend on the chemical composition, reactivity, size, and morphology of the particles as well as on aggregation state, applied concentration, and experimental conditions. Inside living cells, they can interact with crucial processes like oxidative balance, genomic, proteomic, and metabolomic. The nanoparticles can be internalized by endocytosis, and depending on their nature,

Received: June 30, 2017
Revised: August 11, 2017
Accepted: August 17, 2017
Published: August 17, 2017

DOI: 10.1021/acs.jafc.7b03014
J. Agric. Food Chem. 2017, 65, 7874−7884

can be located in different types of organelles. The entrance is controlled by biological and physicochemical attributes such as the cell type, surface chemistry and charge, size, shape, and mechanical properties of the nanoparticles.[18]

Specifically regarding the interaction of nanoparticles and seeds, the literature is still scarce. Table S1[19−27] in the Supporting Information compiles some studies that investigated the effects of Ag, ZnO, Fe, and CuO nanoparticles on seeds. Depending on nanoparticle size, composition, and concentration, germination and root elongation can be either favored or reduced. Studies on Cu-based nanoparticles are even scarcer.

Nanometric copper is broadly used in catalysts, coatings, electronic components, medicines, and lubricant compounds.[28] It means that regardless of their potential application for seed treatment, copper-based nanoparticles will ultimately reach the environment and end up interacting with plants. Therefore, we must investigate and understand how these nanoparticles affect seed germination and seedling development. Albeit found only as a trace element in many plant tissues, copper is considered essential for vegetal life, being a transition metal involved in several metabolic processes like photosynthesis, mitochondrial respiration, oxidative stress protection, and protein synthesis.[29] Nonetheless, most reports in the literature show an increased toxicity in plants exposed to copper nanoparticles. These reports emphasize an inhibitory effect on seedling growth in different species such as black mustard,[30] green peas,[19] mung beans, and wheat.[11]

The present study aimed at investigating the effect of commercial Cu-based nanoparticles, used for seed priming, on the germination and seedling development of *Phaseolus vulgaris*, also known as common bean or kidney bean. In order to verify their potential use as seed fertilizer and the possible high doses impairments, we evaluated the impact of three nanoparticle sizes (25, 40, and <80 nm) at four concentrations (1, 10, 100 and 1 000 mg Cu L^{-1}). Besides monitoring biometric parameters such as germination rate and seedling weight gain, a comprehensive characterization was carried out using X-ray fluorescence (XRF) and X-ray absorption spectroscopy (XAS) seeking to trace the Cu uptake, storage location, and biotransformation.

MATERIALS AND METHODS

Characterization of Pristine CuO Nanoparticles and Dispersions. Copper oxide and passivated CuO nanoparticles (herein all referred as nCuO) were purchased from US Nanomaterials Research Inc. (USA), in three different sizes: 25, 40, and <80 nm. Copper sulfate ($CuSO_4{\cdot}5H_2O$) was purchased from MERCK KGaA (Germany) and used as a copper ionic reference treatment.

The purity of each nCuO was determined by energy dispersive X-ray fluorescence spectroscopy (EDXRF; EDX-720 Shimadzu, Japan). The quantification was carried out using the fundamental parameters method. The procedure of this analysis is described in the Supporting Information. The crystal structure of the nCuO was determined by X-ray diffraction (XRD) employing a PW 1877 diffractometer (Philips, The Netherlands) with Cu−Kα radiation. Through this technique, the crystallite size was evaluated by the Scherrer equation (detailed in the Supporting Information). Nanoparticle morphology was evaluated by scanning electron microscopy (SEM; Inspect F50, FEI Company, USA) at the Brazilian Nanotechnology National Laboratory (LNNano, Campinas, Brazil).

The CuO nanoparticles were suspended in deionized water and dispersed using an ultrasonic processor (model 705 Sonic Dismembrator, Fisher Scientific, USA) under 50% amplitude for 8 min at 1, 10, 100, and 1 000 mg Cu L^{-1}. The hydrodynamic size and the zeta potential were analyzed by dynamic light scattering (DLS; Zetasizer Nano, Malvern Instruments, U.K.) at the Brazilian Biosciences National Laboratory (LNBio, Campinas, Brazil).

Germination Assay. *Phaseolus vulgaris* seeds (common Brazilian bean), variety BRS Cometa, were supplied by the Brazilian Agricultural Research Corporation (EMBRAPA), having an average germination rate of 88%. This seed was chosen as model species because it presents low dormancy, and it results in a plant of small size and short cycle which makes it easy to be employed in laboratory studies. In addition, *P. vulgaris* is an important and accessible source of food.

Seeds were first immersed in a 10% NaClO solution under stirring for 10 s for disinfection, followed by rinsing with deionized water. Subsequently, 20 seeds were soaked for 20 min in the appropriate concentration of each nCuO size. $CuSO_4{\cdot}5H_2O$ solutions at the same concentrations were used as a positive control, whereas deionized water was used as a negative control. After the exposure, the seeds were placed on a 15 cm paper filter fit on the bottom of a Petri dish, and 8 mL of the soaking solution was added for moisturizing the paper filter. The Petri dishes were sealed with Parafilm M (Bemis Company Inc., USA), inserted into a plastic bag for preventing water loss, and finally incubated in a germination chamber (TE-4020, Tecnal, BR) under dark and ventilation at 27 °C for 5 days. The experiment was conducted in quadruplicate per treatment.

The number of germinated seeds was counted daily to determine the rate of germination. After 5 days, the assay was completed. Fresh mass was measured and the germinated seeds were rinsed in deionized water to remove the surface-bound metal or nano metal oxide and then dried in a laboratory oven (515/4A, FANEM, Brazil) at 60 °C for 2 days to obtain the dry mass. The seed weight gain data was submitted to statistical analysis. Once the null hypothesis was rejected in the analysis of variance, we applied Tukey and Dunnett's tests at 95% confidence interval.

Copper Uptake Quantification. Dried seedlings were carefully separated in two fractions: seedling and seed coat. One gram of each component was weighted in a previously decontaminated porcelain crucible and then digested by dry ashing method using a muffle furnace (F-2, Fornitec, Brazil) at 100 °C h^{-1} ramp rate up to 550 °C and ashed for 14 h. Each dry ashing digestion batch included a blank for ensuring no contamination. The ashes were dissolved in 5 mL of 1 M HNO_3(aq), and 950 μL of this solution was transferred into a 1.5 mL vial and 50 μL of 1 000 mg Ga L^{-1} was added as an internal standard. Then, the sample was homogenized using a tube shaker vortex (MA162, Marconi, Brazil).

The Cu content of the digested samples was determined by EDXRF. Procedures and analysis conditions are stated in the Supporting Information.

Mapping the Cu Accumulation Spots. The seeds were exposed to 25 and 80 nm nCuO dispersions at 1 000 mg Cu L^{-1} and 40 nm nCuO at 5 000 mg Cu L^{-1} for 20 min, dried at room temperature, and gently cut in the middle using a stainless steel blade. Subsequently, the seed was placed in a sample holder with a Kapton tape and the cotyledon's inner side exposed for analysis. Chemical images of the primary root were also recorded at the third, fourth, and fifth day of germination. For the latter measurements, the same germination assay procedure was followed, but only the higher nCuO concentration (1 000 mg Cu L^{-1}) treatment and copper sulfate (positive control) were analyzed, except for the 40 nm nCuO treatment which seeds were soaked in 100 mg Cu L^{-1}.

The microanalysis was carried out using a benchtop micro-X-ray fluorescence spectroscopy (μ-XRF) system (Orbis PC EDAX, USA). The Supporting Information presents the experimental setup (Figure S1) and the analysis conditions.

Copper Chemical Speciation Analysis. Sample preparation for determining copper speciation by micro-X-ray absorption near-edge structure (μ-XANES) analysis was the same as used for μ-XRF analysis, but the seeds only received the 1 000 mg Cu L^{-1} dispersion treatment. After drying, the samples were stored in sealed Petri dishes 10 days prior analysis. The analysis was accomplished using μ-XANES at the D09B-XRF beamline at the 1.37 GeV Brazilian Synchrotron Light Laboratory (LNLS, Campinas, Brazil).

DOI: 10.1021/acs.jafc.7b03014
J. Agric. Food Chem. 2017, 65, 7874−7884

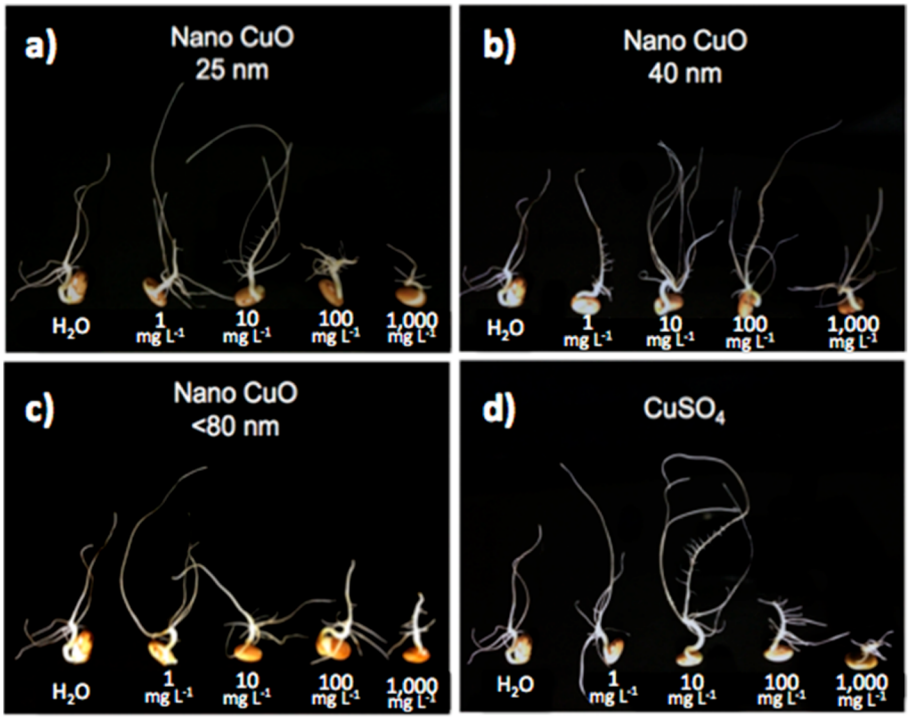

Figure 1. Morphological characteristics of germinated common bean (*Phaseolus vulgaris*) seeds soaked in (a) 25 nm, (b) 40 nm, (c) <80 nm CuO nanoparticles, and (d) $CuSO_4$. Concentrations of the treatments varied from 1 to 1 000 mg Cu L^{-1}.

At XRF beamline, synchrotron radiation was generated by a bending-magnet and collimated by slits. The monochromatic beam was produced by a Si(111) crystal and a KB mirror system was used to focus it to the 20 μm diameter spot size. The μ-XANES was recorded in fluorescence mode using a silicon drift detector (SDD; AXAS-A, KETEK GmbH, Germany). The energy was calibrated utilizing a reference Cu foil.

The chemical maps, previously provided by μ-XRF analysis, aided selecting the proper seed region for μ-XANES analysis according to the Cu accumulation spots after the nCuO exposure. The μ-XRF maps identified three different regions for speciation studies: outside seed coat, within seed coat, and cotyledon near seed coat. The experimental μ-XANES setup is presented in Figure S2 of the Supporting Information.

In order to improve the signal-to-noise ratio, five XANES spectra were recorded and merged in each sample region. Sixteen reference Cu compounds were previously synthesized in our laboratory according to Sarret et al.[31] and measured for providing the model spectra. The μ-XANES spectra were normalized and subjected to linear combination fitting (LCF) analysis using the Athena software of the IFEFFIT package.[32] The uncertainties stated for the weighted compounds correspond to 1σ standard errors.

Root Microscopic Analysis. To determine the exact tissue of Cu accumulation in root samples, seedlings were cleared in a solution of 2.5% commercial bleach in deionized water for 24 h and rinsed in deionized water five times. Roots were cut from the rest of the seedling and mounted on glass slides with 50% glycerol. Images were taken on a Zeiss AxioVert 35 microscope coupled with a Zeiss AxioCam ICc 3 digital camera in brightfield conditions.

Surface Reactivity of CuO Nanoparticles. The reactivity of the CuO nanoparticles was evaluated measuring its ability to decompose H_2O_2 through a Fenton-like reaction.[33] In a 25 mL round-bottom reaction flask, 19.5 mL of a 1 000 mg Cu L^{-1} aqueous dispersion of the tested nanoparticle was magnetically stirred. The flask was connected to a 25 mL graduated pipet through a silicone tube. The pipet was immersed in a measuring cylinder water column. Then, 0.5 mL of 30% v/v H_2O_2 solution was inserted in the reaction flask with a syringe. The volume of the produced O_2 was monitored by following the shift of a water column in a pipet (see the experimental setup at Figure S3 of the Supporting Information). The procedure was carried out twice. In addition to the CuO nanoparticles, also the O_2 evolution by $CuSO_4$ was determined.

RESULTS AND DISCUSSION

Characterization of the Nanoparticles and Dispersions. The purity of the nanoparticles as evaluated by EDXRF (see Table S2 and Figure S4 in the Supporting Information) was above 99.614% for all nanoparticles. As detailed in the Supporting Information, the contaminants found were Cr, Ca, and Sn and their concentrations ranged from hundreds to thousands mg kg^{-1}. XRD patterns, presented in Figure S5 of the Supporting Information, showed that crystalline phases present in the 40 and 80 nm particles corresponded to CuO in the monoclinic phase. For the 25 nm particles, besides the standard diffraction peaks attributed to CuO the XRD pattern also revealed the presence of face centered cubic metallic Cu as informed by the supplier. The crystallite size in the direction of the plane 111 of the oxidic phase was 3.91, 23, and 21 nm for the 25, 40, and 80 nm CuO nanoparticles, respectively. The crystallite size in the 111 direction for the metallic fraction of the 25 nm particles was 5.21 nm (see Table S3). The particle sizes measured by SEM were in agreement with those reported by the supplier (Figure S6).

The stability of the nCuO aqueous dispersions used for seed treatments was evaluated by DLS and zeta-potential (see Table S4 of the Supporting Information). These nanoparticles were dispersed without any surfactants, and primary particle agglomeration was observed with average hydrodynamic diameters of 428, 180, and 273 nm for 25, 40, and 80 nm nCuO, respectively. Measurements showed that these particles presented negative zeta-potentials regardless the size, with values of -21 ± 5, -15 ± 6, and -25 ± 7 mV for 25, 40, and 80 nm nCuO, respectively. The literature reported similar values for 20−200 nm nCuO water dispersions, for which a

DOI: 10.1021/acs.jafc.7b03014
J. Agric. Food Chem. 2017, 65, 7874−7884

hydrodynamic diameter of 480 nm and a zeta potential of −21 ± 2 mV were found.[34]

X-ray absorption spectroscopy (XAS) measurements for the pristine 25 nm nCuO showed that this nanoparticle contained metallic Cu, Cu_2O, and CuO, as shown in Figure S7. The linear combination analysis of the XANES spectra revealed the following proportion: CuO (65 ± 2%), Cu_2O (18 ± 4%), and Cu (17 ± 10%). The XRD input and XAS analysis allowed us to conclude that the structure of the 25 nm nCuO consisted of a metallic core made of Cu covered by oxidized layers of Cu_2O and CuO. Therefore, the results obtained for the 25 nm nCuO may not only be a consequence of their size but may also be influenced by the chemical composition of its core. One should keep in mind that the core properties can affect the surface of the material.

Effects of nCuO on Seed Germination and Seedling Growth. Figure 1 shows the root development on the fifth day after the seeds were exposed to the Cu treatments. Qualitative measurements of growth parameters pointed out that 1 and 10 mg Cu L^{-1} nCuO promoted root elongation in comparison to the water control. Root elongation inhibition was noticed from 100 mg Cu L^{-1} nCuO upward. The only exception was the 100 mg Cu L^{-1} treatment with 40 nm nCuO that did not affect root elongation.

Figure 2 presents both (a) germination rate and (b) fresh mass gain on day 5 after germination. For the water control, the average germination rate was 80%. All the nCuO treated seeds had higher or comparable values compared to the negative control, except for the 40 nm nCuO treatment at 1 mg Cu L^{-1} that had only 70% germination. The highest and the lowest germination rates were found for the $CuSO_4$ treatments at 100 (92.5%) and 1 000 mg Cu L^{-1} (65%), respectively.

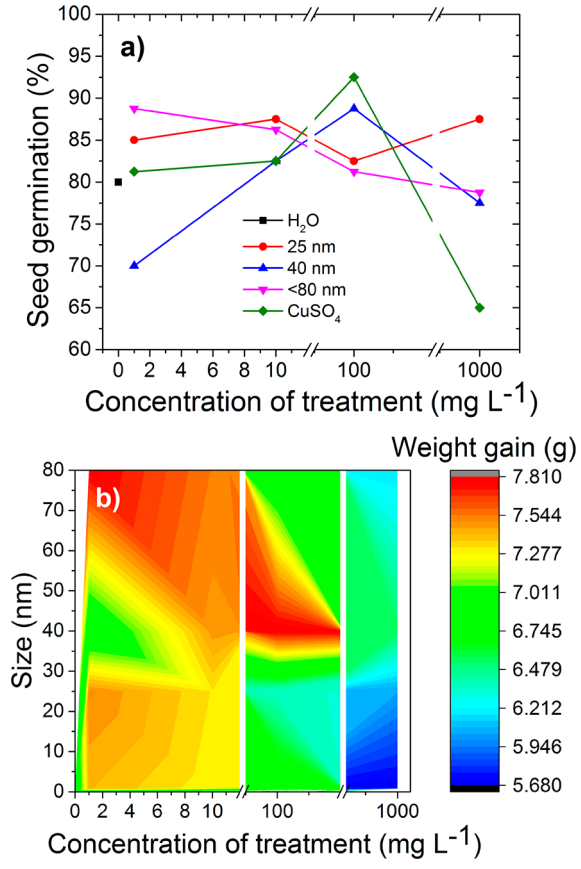

Figure 2. (a) Germination rate and (b) fresh mass gain of common bean (*Phaseolus vulgaris*) seeds exposed to 25, 40, <80 nm CuO nanoparticles, $CuSO_4$ (1−1 000 mg Cu L^{-1}), and H_2O (control) after 5 days of germination.

Figure 2b displays the fresh weight gain in a 2D plot as a function of the concentration of Cu in the dispersion and particle size. For the negative control (water), we considered zero entry values for particle size and concentration. For the positive control ($CuSO_4$), we considered a size of 0.8 nm based on the diameter of $CuSO_4$ molecule[35] and the several concentrations employed in the test. The 2D plot interpolates sizes and concentrations revealing the trends between the actual tested points. Figure 2b shows that on the fifth day of the germination assay, some treatments tended to promote fresh mass gain (reddish areas) whereas others tended to prevent it (bluish areas). Seeds exposed to 80 and 40 nm nCuO at 1 and 100 mg Cu L^{-1}, respectively, had the highest mass gain. The 25 nm CuO nanoparticles were deleterious at 100 and 1 000 mg Cu L^{-1}, while the <80 nm nCuO and $CuSO_4$ reduced seedling development at 1 000 mg Cu L^{-1}. The difference between the higher and lower mass gain was statistically significant according to the Tukey test ($p < 0.05$). Figure S8 shows that low concentrations and higher particle size improved mass gain whereas higher concentrations regardless of the particle size, including $CuSO_4$, reduced the mass gain. A similar trend was found for the dry mass (data not shown here).

The mass gain test suggested a hormetic behavior for 40 nm CuO particles reaching the maximum beneficial effect at 100 mg Cu L^{-1}. According to the Dunnett's test, mass gain was significantly different from the control at 100 mg Cu L^{-1} of 40 nm nCuO and for $CuSO_4$ at 1 000 mg Cu L^{-1} (Figure S9). Among the nanoparticles, mass gain showed a dose-related decrease for 25 nm CuO, with the inhibition being similar to that of $CuSO_4$ at 1 000 mg Cu L^{-1}.

Copper is a micronutrient, but as any chemical it becomes toxic at high concentrations. High Cu concentrations reduce root development, leading to deficient water and nutrient uptake and consequent growth reduction.[36] This was confirmed by the results shown in Figure 1, where seedling growth is strongly affected by an excess of Cu.

Increments in germination rate were also observed for other seed species treated with nano Zn[23] and Ag.[20] Gokak and Taranath suggested that Zn nanoparticles may photo generate radical species that can favor the germination process, Parveen and Rao argued that Ag nanoparticles might create nano holes facilitating the water transport. Although these hypotheses might sound interesting, the experimental strategies in the cited papers did not prove them. The argument that the radical, regardless the generation mechanism, found some resonance in our results. As discussed below, the copper nanoparticles were reactive (in terms of H_2O_2 decomposition), it is currently known that radicals may also act as singling molecule and therefore, under certain conditions, they could promote the germination.[37]

Contrary to our findings, low doses of <50 nm CuO nanoparticles decreased the germination of rice (*Oryza sativa* L.); the concentrations used were 0.5−1.5 mM (39.8 to 119.3 mg L^{-1}). Root mass and length were equally affected under nCuO stress. Copper stressed roots showed loss of viable cells as established by Evans blue staining.[38] In green peas (*Pisum sativum* L.), mass gain was also impaired at higher nCuO concentrations (from 100 to 500 mg L^{-1}). An increase in

DOI: 10.1021/acs.jafc.7b03014
J. Agric. Food Chem. 2017, 65, 7874−7884

reactive oxygen species, lipid peroxidation, and gene expression in the roots were found.[19] Lower concentrations (10 and 20 mg L^{-1}) of 20−30 nm nCuO reduced the root length and mass gain of lettuce (*Lactuca sativa*), accompanied by increased catalase activity and decreased ascorbate peroxidase activity.[39]

Thus, in addition to our results that showed that dose and type of nanoparticles play a role in the seed germination and growth effects, the literature indicated that the effects may also vary from one plant species to another.

Determination of Cu Uptake by *Phaseolus vulgaris* Seeds. To determine the Cu content of seedlings exposed to nCuO, $CuSO_4$, and water by EDXRF, the seed coat was removed to enable separate analysis of the seedling and respective seed coat (Figure S10 in the Supporting Information).

Figure 3 presents the concentration of Cu accumulated in the seedlings (a) and in the seed coat (b). The concentration of Cu

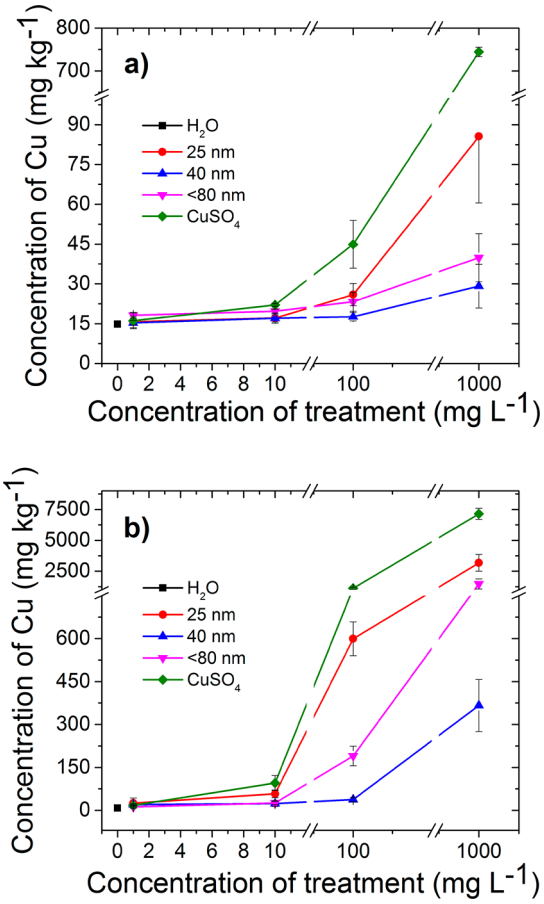

Figure 3. Copper concentrations in the (a) seedling and (b) seed coat of germinated common bean (*Phaseolus vulgaris*) seeds treated with 25, 40, <80 nm CuO nanoparticles, $CuSO_4$ (1−1 000 mg Cu L^{-1}) and H_2O (control).

in both the seedling and the seed coat increased as a function of the nCuO or $CuSO_4$ concentration. Copper was much more concentrated in the external than in the inner part of the seeds. It means that the seed coat was an effective barrier for nCuO absorption, but this was less the case for $CuSO_4$. In the case of ZnO nanoparticles, Zn uptake by the endosperm of corn without seed coat during germination was about six times higher than in the whole grain.[22]

Deionized water treatment (negative control) gave concentrations of 14.8 ± 0.5 mg Cu kg^{-1} in the seedling and 8.2 ± 1.6 mg Cu kg^{-1} in the seed coat. Concentrations close to the negative control were observed for the seeds exposed to nCuO at 1 and 10 mg Cu L^{-1}, suggesting that at these concentrations Cu hardly managed to enter and cross the seed coat. The concentration of Cu incorporated by the seeds sharply rose at nCuO exposure levels of 100 and 1 000 mg Cu L^{-1}. Compared to the other two nanoparticles sizes, the 40 nm nCuO seemed to be less incorporated by the seeds.

A linear correlation was found between the concentration of Cu taken up by the seed coat and seedling and the $CuSO_4$ concentration of the solution used for seed priming. Both adjusts (not shown here) gave Pearson's $r > 0.98$. The slope for the relationship between Cu concentration in the embryo and exposure concentration (Figure 3a) was 11.2 times lower than that found for the seed coat (Figure 3b).

Cu solubility tests carried out to evaluate the fraction of soluble Cu ions released by the nCuO (see Figure S11) indicated that the smaller the nCuO size, the greater the solubility. At 100 mg Cu L^{-1}, the supernatant fraction of the 25 nm nCuO dispersion contained 1.1 ± 0.3 mg Cu L^{-1} compared with 0.18 ± 0.01 mg Cu L^{-1} for the 80 nm nCuO dispersion. Such low concentrations in solution suggest that Cu incorporated by the seedling corresponded mainly to dispersed nCuO rather than only to ionic Cu in solution. For cucumber seedlings (*Cucumis sativus* L.), which seeds were exposed to ZnO nanoparticles, the Zn content was significantly correlated with the soluble Zn found in the solution, which indicates that cucumber seeds uptake Zn mainly in the soluble form.[22]

Exposure to the 80 nm nCuO led to concentrations of 40 ± 9 and 1 500 ± 400 mg Cu kg^{-1} in the embryo and seed coat, respectively. Different from the 25 nm nCuO, no effect on germination or weight was found for 80 nm nCuO at 1 000 mg Cu L^{-1}. These results suggest that these latter nanoparticles may be used in seed priming when it is aimed at overcoming Cu deficiency.

Spatial Distribution of Cu in the Soaked Seeds. μ-XRF is a nondestructive microanalytical method that allows evaluating the spatial distribution of elements in for instance biological tissues. To the best of our knowledge, this is the first μ-XRF mapping of treated seeds. This technique has been commonly used to investigate the allocation of elements in nontreated seeds like wheat,[40] rice,[41] soybean,[42] and *Arabidopsis thaliana*.[43] However, most of these studies employed synchrotron X-ray sources. Here we show results acquired using an X-ray tube excitation laboratory benchtop facility that uncovered the pattern of distribution of Cu in the nCuO and $CuSO_4$ exposed bean seeds.

Figure 4 shows the mapped area of the seed and the corresponding Cu chemical image for a seed soaked in $CuSO_4$ (a) nCuO 25 nm (b) and nCuO 40 nm (c). The seeds were soaked in solutions of $CuSO_4$, nCuO 25 and 80 nm at 1 000 mg Cu L^{-1} (shown in Figure S12), and 40 nm nCuO at 5 000 mg Cu L^{-1} for 20 min. Additional pictures and chemical images for potassium are presented in Figures S12−S14 of the Supporting Information. The images in Figure 4 and Figures S12−S14 were recorded 24 h after the soaking and prior to seed germination. The μ-XRF maps confirmed the EDXRF results (shown above) that the Cu was mostly concentrated in the seed coat but also revealed the presence of Cu hotspots in the hilum region.

DOI: 10.1021/acs.jafc.7b03014
J. Agric. Food Chem. 2017, 65, 7874−7884

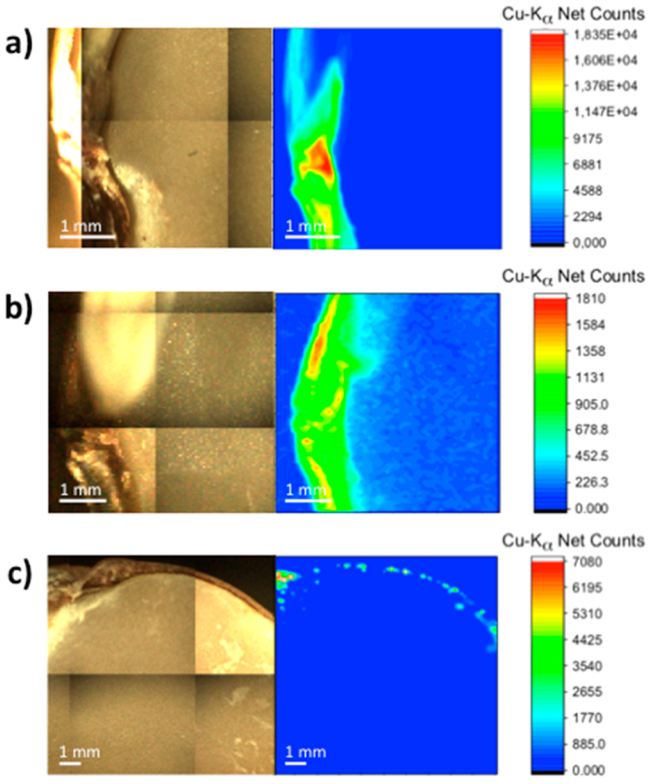

Figure 4. Pictures and μ-XRF chemical maps for Cu in common bean (*Phaseolus vulgaris*) seeds exposed to (a) $CuSO_4$ at 1 000 mg Cu L^{-1}, (b) nano CuO 25 nm at 1 000 mg Cu L^{-1}, and (c) nano CuO 40 nm at 5 000 mg Cu L^{-1}.

To be absorbed by the seeds, the water-dispersed nanoparticle must cross the seed coat (or testa). This structure is composed by a layer of sclerenchyma cells, similar to the palisade cells, with a thick cell wall. Below this layer, there is another layer characterized by smaller cells and finally a parenchyma composed of elongated outer cells and smaller internal cells with irregular or branched shapes. Common beans have a hilum associated with the seed coat, which is a scar left by the funiculus, the structure that connects the seed to the placenta. Just below the hilum there is the micropyle, a small pore that allows water uptake into the seed.[44]

The chemical images also revealed the existence of a concentration gradient from the outer to the inner region of the seed. This indicates that movement of Cu is driven by the higher chemical potential of the nCuO dispersion or $CuSO_4$ solution. Since the seed coat is not a homogeneous structure, the nCuO particles or Cu ions may find preferential channels, such as through the micropyle.

Different from the EDXRF assessment, which gave the average concentrations of Cu in the seedling (comprising the storage tissue and emerging root) (Figure 3a), the spatial resolution provided by the 30 μm X-ray beam shows that Cu is concentrated in a small fraction of the embryo. Therefore, although Cu is not well distributed along the seedling tissue, its presence in very specific regions of the tissue was sufficient to affect seedling weight gain at 1 000 mg Cu L^{-1}.

Because of its high solubility, Cu from the $CuSO_4$ treatment was more prone to be absorbed than from the nCuO treatment. This indicates that Cu transport through the seed occurs by diffusion, since the transport of Cu ions is much faster and easier than that of nanoparticles.

Chemical Speciation of the Incorporated Cu. Once Cu accumulation spots were located, we determined its chemical speciation using XAS, which is a nondestructive tool. Figure 5a shows the spots measured in the treated seeds, the specific locations measured for each treated seed are presented in Figures S15–S17 in the Supporting Information. Figure 5b–d

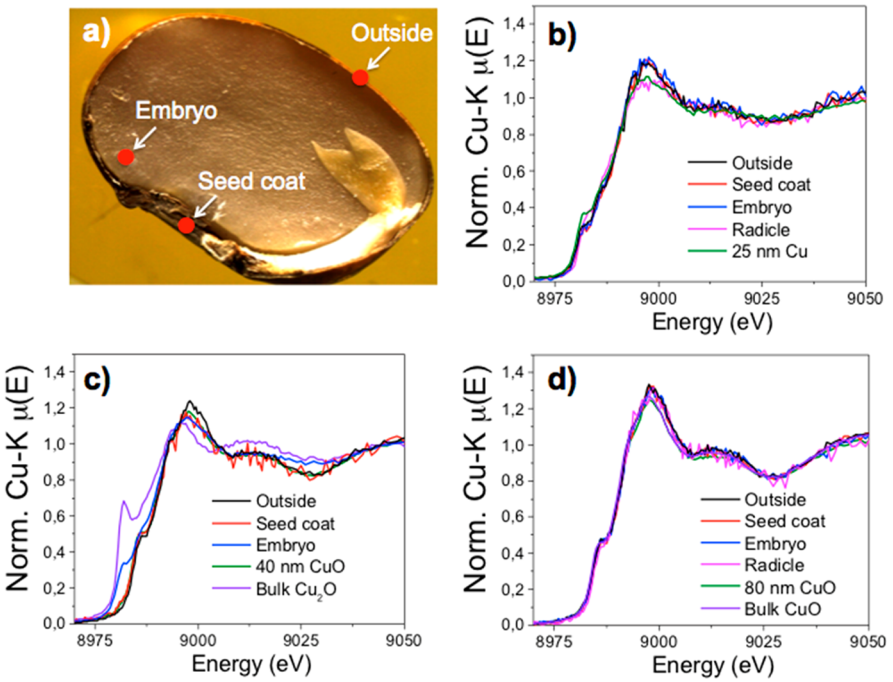

Figure 5. Cu–K edge XAS spectra recorded in different regions of bean (*Phaseolus vulgaris*) seeds treated with 1 000 mg Cu L^{-1} dispersions of CuO nanoparticles. (a) Picture of a bean seed pointing out the three regions measured, (b) spectra recorded of the 25 nm nCuO treatment, (c) spectra recorded of the 40 nm nCuO treatment, and (d) spectra recorded of the 80 nm nCuO treatment.

DOI: 10.1021/acs.jafc.7b03014
J. Agric. Food Chem. 2017, 65, 7874–7884

shows the spectra recorded in the outside, seed coat, embryo, radical, and pristine nanoparticles used to produce the 1 000 mg Cu L^{-1} dispersions. Figure 5b presents data for treatments with 25 nm nCuO, Figure 5c for 40 nm nCuO and Figure 5d for 80 nm nCuO.

Figure 5b indicates that the chemical environment on the outside of the seed coat, in the hilum region (seed coat) and inside the seed (embryo) treated with 25 nm nCuO was the same. The spectra recorded in these regions are slightly different from the spectra obtained for the pristine 25 nm nCuO. The observed differences are the decrease of the pre-edge feature at 8 982 eV assigned to the 1s to 4p electronic transition in Cu^{1+} followed by an increase of the white line intensity. These two spectral changes are related to the oxidation of Cu^{1+} to Cu^{2+}.[45] The spectrum recorded in the radical presented the features of the pristine material.

Figure 5c shows a pronounced pre-edge feature for the Cu located in the embryo of the seed primed with nCuO. This feature is associated with Cu^{1+} and indicates that 40 nm nCuO was reduced compared to that found in the seed coat and outside of the seed. The linear combination analysis (Figure S18) showed that spectra recorded in the embryo could be described as a mixture of 34 ± 1% Cu_2O and 66 ± 1% CuO. Figure 5d shows that the chemical neighborhood of Cu incorporated by the seed tissues and radical in the samples treated with 80 nm nCuO did not change and remained as CuO. The spectra recorded in the samples perfectly overlapped that recorded for the pristine 80 nm nCuO powder.

The copper chemical environment in harvested *Arabidopsis thaliana* seeds treated with 20 and 50 mg L^{-1} nCuO was also mostly in the form of CuO (88.8%), with some $Cu_2(OH)PO_4$ (2.0%), Cu-acetate (3.2%), and Cu_2O (6.0%).[48] This suggests that nCuO can be also accumulated in plant progeny.

Although our results showed a slight redox behavior for 40 and 25 nm nCuO in a physiological environment, the Cu-based nanoparticles used in this study were not as reactive as ZnO.[40] This can be partially explained by the low solubility of the CuO based nanoparticles. However, one has to keep in mind that the sensitivity of XAS would hardly be able to identify the presence of Cu factions below 5 wt %.

The combined data supplied by EDXRF, μ-XRF maps, μ-XANES, and literature background on seed morphology[44] suggested that the main Cu uptake mechanism takes place through diffusion driven by the concentration gradient. The main entrance region was the hilum spongy tissue. The presence of CuO and Cu_2O most likely indicated that the CuO nanoparticles were incorporated as entire particles instead of anions. In addition to the spectroscopic speciation, this hypothesis was supported by the hilum pore size, which reaches tens of micrometers (Figure S19). The presence of Cu in the endosperm region away from the hilum (Figure 4c) also implied that possibility of Cu to cross the seed coat structure. Nevertheless, the extent of the penetration into the endosperm was smaller. In this context, it is worth mentioning that there are many pathways of Cu transportation in plants. In cell-to-cell migration, Cu can be coordinated by proteins like Cu chaperones and Cu carriers, which transport Cu to the organelles.[47]

***In Vivo* Spatial Distribution of Cu in the Seedlings.** In addition to the chemical maps that uncovered the spatial distribution of Cu in the seeds after the priming, we mapped the *in vivo* chemical distribution of Cu in the primary root of the seedling under development. We monitored seedlings primed in $CuSO_4$ at 1 000 mg Cu L^{-1} and 40 nm nCuO at 100 mg Cu L^{-1} since these treatments showed significant effects compared to the control according to the Dunnett's test.

Figure 6a–c shows the pictures and corresponding Cu–Kα chemical images for the emerging primary root of the seedling

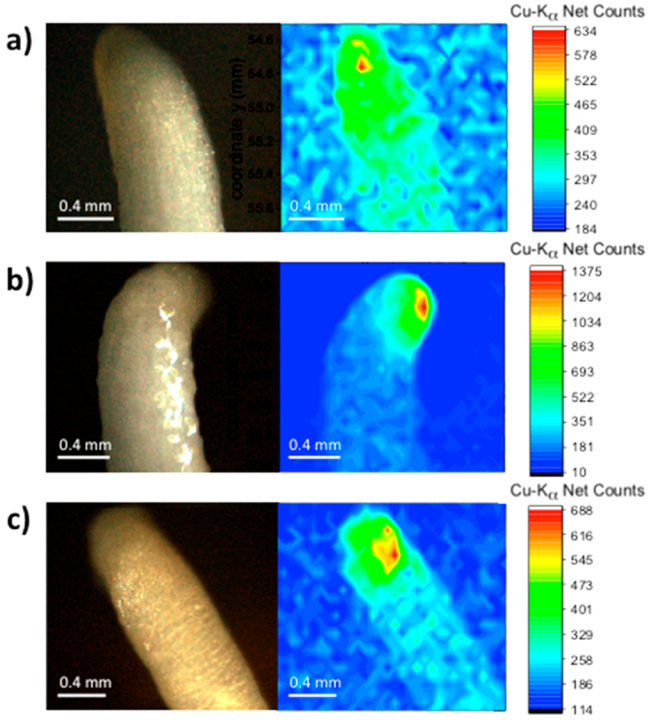

Figure 6. Pictures and μ-XRF chemical maps for Cu in the primary root of a common bean (*Phaseolus vulgaris*) seed exposed to $CuSO_4$ at 1 000 mg Cu L^{-1} on the (a) third, (b) fourth, and (c) fifth day of germination.

primed in $CuSO_4$ at 1 000 mg Cu L^{-1} on the third, fourth, and fifth day of germination, respectively. The chemical images revealed a hotspot of Cu on the tip of the primary root, which remained on the same location along the monitored period and was not diluted during the growing process.

Figure 7 presents the pictures and chemical maps for the tip of the primary root of the seedling treated with 40 nm nCuO at 100 mg Cu L^{-1} on the third (a), fourth (b), and fifth (c) day of the seedling growth. The results were similar to those found for $CuSO_4$.

Figure 8 presents an optical microscope image that was allowed to precisely identify the tissue in which the Cu spots were found. It corresponded to the root cap. We believe that the root cap incorporated Cu from the seed coat during the radical emergence. It is also noteworthy mentioning that the incorporation and diffusion of Cu could be favored by the chemical properties of mucilage, especially in the soluble form. The chemical images also showed that the Cu transferred to the root cap had low mobility. Part of the Cu could have been transferred to the meristem, site of intense cell division activity, which at low concentrations may have favored root growth while at high concentration it might have prevented it. Previous experiments carried out by Wang and colleagues, in the model species *Arabidopsis thaliana*, showed that nCuO treatments induce modulation of auxin related genes, supporting the idea that changes in root growth rates are related to the modulation of auxin sensing and root size control.

DOI: 10.1021/acs.jafc.7b03014
J. Agric. Food Chem. 2017, 65, 7874–7884

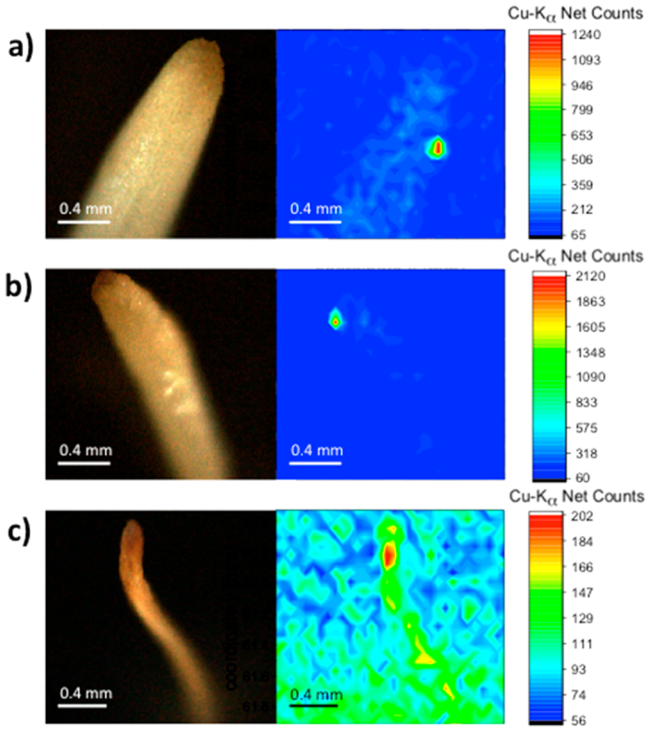

Figure 7. Pictures and μ-XRF chemical maps for Cu in the primary root of a common bean (*Phaseolus vulgaris*) seed exposed to nano CuO 40 nm at 100 mg Cu L^{-1} on the (a) third, (b) fourth, and (c) fifth day of germination.

Chemical Reactivity of Cu Based Nanoparticles and Physiological Effects. The deleterious effects of the 25 nm CuO nanoparticles at 100 and 1 000 mg Cu L^{-1} could not be explained by the treatment concentration, since a different behavior was found for 40 and 80 nm nCuO. The crystal phase effects could not be accessed in the present study since for all particles the CuO were monoclinic. However, the literature indicated that for rutile and anatase TiO_2 the crystal phase did not influence the uptake and translocation of TiO_2 in wheat.[46]

Figure S20 shows the degradation of H_2O_2 by the CuO nanoparticle dispersions used to prime the seeds. The 40 and 80 nm nCuO presented similar behavior, taking nearly 300 min to produce 7.9 and 8.5 mL of O_2, respectively. $CuSO_4$ produced 18.5 mL of O_2 in 180 min. The most reactive nanoparticle was the 25 nm CuO that readily produced 18.5 mL of O_2 in 30 min. The surface properties of core−shell structures can greatly differ from those exhibited by single phase materials. For example, the catalytic activity of Ru−Cu nanoparticles in converting NH_3 into N_2 and H_2 depends on the number of Cu layers on top of Ru.[49] Facing the low solubility shown by all Cu-based nanoparticles used in the present study and the similar results obtained for the 40 and 80 nm CuO particles, we hypothesize that the deleterious effects of the 25 nm particles may be caused by their modified surface properties.

Considering the excess of Cu ions, the deleterious effects can be explained in the light of previous studies. The literature reports after 5 days of germination under normal conditions, an increase in protein and amino acid content in *Phaseolus* beans.[50] On the other hand, cotyledons of germinating bean seeds (*Phaseolus vulgaris*) exposed to 200 μM $CuCl_2$ (26.9 mg L^{-1}) showed protein damage and oxidative stress. In common beans, Cu toxicity caused inactivation of the ubiquitin-proteasome pathway, an important nonlysosomal proteolytic system, and inhibition of leucine and proline aminopeptidase activities. These injuries led to a deficiency in the cell's capability to remove oxidatively damaged proteins.[51] Oxidative stress was also found in lettuce treated with nCuO at 20 mg L^{-1}. Cu reduced catalase and ascorbate peroxidase activities, two important antioxidant enzymes.[39] Nevertheless, our chemical speciation did not detect Cu binding to proteins. The chemical environments were mostly similar to those of pristine materials. It means that in the case Cu−protein interaction actually happened, the fraction of Cu playing this role was below the XAS detection limit. In linear combination analysis of XAS, a component weighting less than 5% would be hardly detectable, since normalization can introduce errors on the order of 10%.

Besides preventing the development of *P. vulgaris*, Cu based treatments led to reduction of the content of Ca, Fe, K, Mn, Zn, carbohydrates, and amino acids as was also observed in the embryonic axis of seeds exposed to excess Cu (5 mmol L^{-1} or 672.2 mg L^{-1} of $CuCl_2$). Oxidative damage may be enhanced in Cu-intoxicated tissues and affect membrane integrity due to the lipid peroxidation process, which induces solute leakage from germinating seeds.[52]

Chemical imaging combined with spectroscopic speciation showed that although Cu was located in small hotspots instead of being spread homogeneously throughout the tissues, and most of the incorporated Cu remained in its pristine form, it strongly affected the germination of the seeds and the growth of the seedlings. As discussed above, it is likely that low concentrations of promptly available Cu ions may have impaired the proper functioning of proteins.

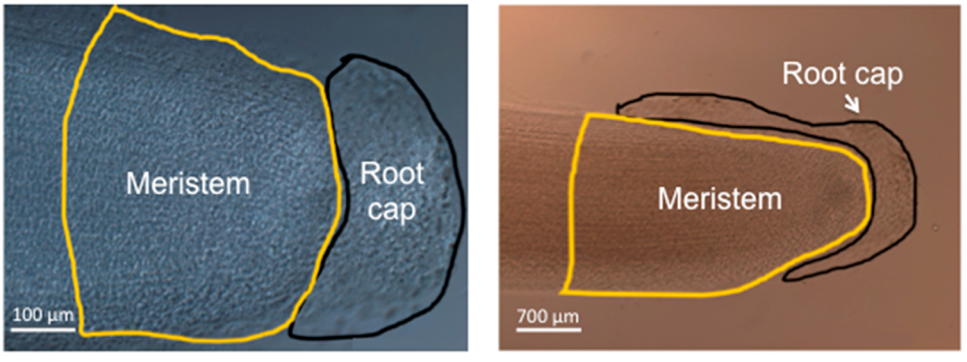

Figure 8. Optical microscopy of primary roots of the common bean *Phaseolus vulgaris*. The root cap is the site that contained the highest Cu concentrations after exposure of the beans to CuO nanoparticles or $CuSO_4$.

DOI: 10.1021/acs.jafc.7b03014
J. Agric. Food Chem. 2017, 65, 7874−7884

In agreement to the published literature, the present study shows that much attention has to be paid to the concentration of the nanoparticles used in seed priming. At concentrations from 1 to 100 mg Cu L^{-1}, 40 and 80 nm nCuO did not harm the seed germination and seedling development, while 40 nm nCuO at 100 mg Cu L^{-1} favored weight gain. The 80 nm nCuO did not affect weight gain, although it was able to increase concentrations in the embryo to 40 ± 9 mg Cu kg^{-1}. This might be a consequence of the slow release of Cu ions from the oxide structure to the physiological solution. Therefore, Cu in these oxide forms can be used by the developing seedling instead of intoxicating it, different from what happened for $CuSO_4$ at 1 000 mg Cu L^{-1} which prevented seedling growth. Hence, depending on its physical-chemical properties, CuO based nanoparticles might be considered for seed priming rather than soluble Cu sources, since the possibility of phytotoxicity by the latter is higher.

The current study also highlighted the importance of the structure and chemical nature of the nanoparticle. The effects of 25 nm nCuO, which presented a metallic core covered by an oxide shell structure, deserve further investigation. This nanoparticle, probably due to its higher surface reactivity, had deleterious effects on bean seedling development. These results reinforce the necessity of care regarding the disposal of nanoparticles in the environment and their usage as fertilizers.

■ ASSOCIATED CONTENT

Supporting Information

The Supporting Information is available free of charge on the ACS Publications website at DOI: 10.1021/acs.jafc.7b03014.

Bibliographic survey of nanoparticle seed treatment; μ-XRF experimental setup and additional bean seeds chemical images; μ-XANES experimental setup; experimental setup and results for the nCuO reactivity analysis; purity and contaminant analysis of each nCuO (EDXRF methodology, quantitative results, and spectra); diffractograms and crystallite size of each nCuO provided by the XRD analysis; SEM images of each nCuO; zeta potential and hydrodynamic diameter of the nCuO dispersions determined by DLS; XAS spectra recorded for the 25 nm nCuO; statistical analysis (Tukey and Dunnett tests); pictures of the two fractions of the seedlings (seedling and seed coat) analyzed by EDXRF; nCuO solubility (methodology and quantitative results); pictures of the specific regions of the bean seeds in which the μ-XANES spectra were recorded; XAS spectra recorded in the embryo of a bean seed treated with 40 nm nCuO at 1 000 mg Cu L^{-1}; and surface reactivity of nCuO (PDF)

■ AUTHOR INFORMATION

Corresponding Author

*E-mail: hudson@cena.usp.br. Phone: + 55 19 3429 4737.

ORCID

Hudson W. Pereira de Carvalho: 0000-0003-0875-3261

Funding

This study was supported by FAPESP Young Investigators Award 2015/05942-0 and the FAPESP Multiuser Equipment Program Grant 2015/19121-8. CAPES (Coordination for the Improvement of Higher Education Personnel) is acknowledged for granting a scholarship to N.M.D., and S.M.S. was supported by the CNPq (National Council for Scientific and Technological Development).

Notes

The authors declare no competing financial interest.

■ ACKNOWLEDGMENTS

The authors are grateful for the LNNano and LNBio facilities. We thank LNLS for beamtime at XRF beamline (Proposal 20160076) and the beamlines scientists, Dr. Carlos A. Perez and Dr. Douglas Galante, for their support during the XAS measurements. EMPRAPA is also acknowledged for the supplied *Phaseolus vulgaris* seeds, variety BRS Cometa. We are also grateful to the technician Monica L. Rossi for the root clearing and microscopy preparations.

■ ABBREVIATIONS USED

CeO_2, cerium dioxide; $Cu_2(OH)PO_4$, copper(II) hydroxide phosphate; Cu_2O, copper(I) oxide; CuO, copper(II) oxide; $CuSO_4$, copper sulfate; DLS, dynamic light scattering; EDXRF, energy dispersive X-ray fluorescence spectroscopy; H_2O, water; LCF, linear combination fitting; LNBio, Brazilian Biosciences National Laboratory; LNLS, Brazilian Synchrotron Light Laboratory; LNNano, Brazilian Nanotechnology National Laboratory; nCuO, copper oxide nanoparticles; SDD, silicon drift detector; SEM, scanning electron microscopy; TiO_2, titanium dioxide; XAS, X-ray absorption spectroscopy; XRD, X-ray diffraction; XRF, X-ray fluorescence spectroscopy; ZnO, zinc oxide; μ-XANES, micro-X-ray absorption near-edge structure; μ-XRF, micro-X-ray fluorescence spectroscopy

■ REFERENCES

(1) Borm, P. J.; Robbins, D.; Haubold, S.; Kuhlbusch, T.; Fissan, H.; Donaldson, K.; Schins, R.; Stone, V.; Kreyling, W.; Lademann, J.; Krutmann, J.; Warheit, D.; Oberdorster, E. The potential risks of nanomaterials: a review carried out for ECETOC. *Part. Fibre Toxicol.* **2006**, *3*, 11.

(2) EFSA Scientific Committee. Guidance on the risk assessment of the application of nanoscience and nanotechnologies in the food and feed chain. *EFSA J.* **2011**, *9*, 2140.

(3) RIKILT and JRC. Inventory of Nanotechnology applications in the agricultural, feed and food sector. *EFSA Supporting Publication* **2014**, EN-621

(4) Dasgupta, N.; Ranjan, S.; Ramalingam, C. Applications of nanotechnology in agriculture and water quality management. *Environ. Chem. Lett.* **2017**, DOI: 10.1007/s10311-017-0648-9.

(5) Pedrini, S.; Merritt, D. J.; Stevens, J.; Dixon, K. Seed coating: science or marketing spin? *Trends Plant Sci.* **2017**, *22*, 106−116.

(6) Farooq, M.; Wahid, A.; Siddique, K. H. M. Micronutrient application through seed treatments - a review. *J. Soil Sci. Plant Nut.* **2012**, *12*, 125−142.

(7) Farooq, M.; Basra, S. M. A.; Wahid, A.; Khaliq, A.; Kobayashi, N. Rice seed invigoration. In *Sustainable Agriculture Reviews*; Lichtfouse, E., Ed.; Springer: The Netherlands, 2009; pp 137−175.

(8) Malhi, S. S. Effectiveness of seed-soaked Cu, autumn- versus spring-applied Cu, and Cu-treated P fertilizer on seed yield of wheat and residual nitrate-N for a Cu-deficient soil. *Can. J. Plant Sci.* **2009**, *89*, 1017−1030.

(9) Cifuentes, Z.; Custardoy, L.; de la Fuente, J. M.; Marquina, C.; Ibarra, M. R.; Rubiales, D.; Perez-De-Luque, A. Absorption and translocation to the aerial part of magnetic carbon-coated nanoparticles through the root of different crop plants. *J. Nanobiotechnol.* **2010**, *8*, 26.

(10) Larue, C.; Castillo-Michel, H.; Sobanska, S.; Cecillon, L.; Bureau, S.; Barthes, V.; Ouerdane, L.; Carriere, M.; Sarret, G. Foliar exposure of the crop *Lactuca sativa* to silver nanoparticles: Evidence

for internalization and changes in Ag speciation. *J. Hazard. Mater.* **2014**, *264*, 98−106.
(11) Lee, W. M.; An, Y. J.; Yoon, H.; Kweon, H. S. Toxicity and bioavailability of copper nanoparticles to the terrestrial plants mung bean (*Phaseolus radiatus*) and wheat (*Triticum aestivum*): Plant agar test for water-insoluble nanoparticles. *Environ. Toxicol. Chem.* **2008**, *27*, 1915−1921.
(12) Prasad, T.; Sudhakar, P.; Sreenivasulu, Y.; Latha, P.; Munaswamy, V.; Reddy, K. R.; Sreeprasad, T. S.; Sajanlal, P. R.; Pradeep, T. Effect of nanoscale zinc oxide particles on the germination, growth and yield of peanut. *J. Plant Nutr.* **2012**, *35*, 905−927.
(13) Lopez-Moreno, M. L.; de la Rosa, G.; Hernandez-Viezcas, J. A.; Castillo-Michel, H.; Botez, C. E.; Peralta-Videa, J. R.; Gardea-Torresdey, J. L. Evidence of the differential biotransformation and genotoxicity of ZnO and CeO_2 nanoparticles on soybean (*Glycine max*) plants. *Environ. Sci. Technol.* **2010**, *44*, 7315−7320.
(14) Morales, M. I.; Rico, C. M.; Hernandez-Viezcas, J. A.; Nunez, J. E.; Barrios, A. C.; Tafoya, A.; Flores-Marges, J. P.; Peralta-Videa, J. R.; Gardea-Torresdey, J. L. Toxicity assessment of cerium oxide nanoparticles in cilantro (*Coriandrum sativum L.*) plants grown in organic soil. *J. Agric. Food Chem.* **2013**, *61*, 6224−6230.
(15) Lopez-Moreno, M. L.; de la Rosa, G.; Hernandez-Viezcas, J. A.; Peralta-Videa, J. R.; Gardea-Torresdey, J. L. X-ray absorption spectroscopy (XAS) corroboration of the uptake and storage of CeO_2 nanoparticles and assessment of their differential toxicity in four edible plant species. *J. Agric. Food Chem.* **2010**, *58*, 3689−3693.
(16) Frazier, T. P.; Burklew, C. E.; Zhang, B. H. Titanium dioxide nanoparticles affect the growth and microRNA expression of tobacco (*Nicotiana tabacum*). *Funct. Integr. Genomics* **2014**, *14*, 75−83.
(17) Tan, W. J.; Du, W. C.; Barrios, A. C.; Armendariz, R.; Zuverza-Mena, N.; Ji, Z. X.; Chang, C. H.; Zink, J. I.; Hernandez-Viezcas, J. A.; Peralta-Videa, J. R.; Gardea-Torresdey, J. L. Surface coating changes the physiological and biochemical impacts of nano-TiO_2 in basil (*Ocimum basilicum*) plants. *Environ. Pollut.* **2017**, *222*, 64−72.
(18) Mu, Q. X.; Jiang, G. B.; Chen, L. X.; Zhou, H. Y.; Fourches, D.; Tropsha, A.; Yan, B. Chemical basis of interactions between engineered nanoparticles and biological systems. *Chem. Rev.* **2014**, *114*, 7740−7781.
(19) Nair, P. M. G.; Chung, I. M. The responses of germinating seedlings of green peas to copper oxide nanoparticles. *Biol. Plant.* **2015**, *59*, 591−595.
(20) Parveen, A.; Rao, S. Effect of nanosilver on seed germination and seedling growth in *Pennisetum glaucum*. *J. Cluster Sci.* **2015**, *26*, 693−701.
(21) Thuesombat, P.; Hannongbua, S.; Akasit, S.; Chadchawan, S. Effect of silver nanoparticles on rice (*Oryza sativa L.* cv. KDML 105) seed germination and seedling growth. *Ecotoxicol. Environ. Saf.* **2014**, *104*, 302−309.
(22) Zhang, R. C.; Zhang, H. B.; Tu, C.; Hu, X. F.; Li, L. Z.; Luo, Y. M.; Christie, P. Phytotoxicity of ZnO nanoparticles and the released Zn(II) ion to corn (*Zea mays* L.) and cucumber (*Cucumis sativus* L.) during germination. *Environ. Sci. Pollut. Res.* **2015**, *22*, 11109−11117.
(23) Gokak, I. B.; Taranath, T. C. Morphological and biochemical responses of *Abelmoschus esculantus* (L.) Moench to zinc nanoparticles. *Adv. Nat. Sci.: Nanosci. Nanotechnol.* **2015**, *6*, 025017.
(24) Li, X.; Yang, Y. C.; Gao, B.; Zhang, M. Stimulation of peanut seedling development and growth by zero-valent iron nanoparticles at low concentrations. *PLoS One* **2015**, *10*, e0122884.
(25) Xiang, L.; Zhao, H. M.; Li, Y. W.; Huang, X. P.; Wu, X. L.; Zhai, T.; Yuan, Y.; Cai, Q. Y.; Mo, C. H. Effects of the size and morphology of zinc oxide nanoparticles on the germination of Chinese cabbage seeds. *Environ. Sci. Pollut. Res.* **2015**, *22*, 10452−10462.
(26) Nair, P. M. G.; Chung, I. M. Physiological and molecular level studies on the toxicity of silver nanoparticles in germinating seedlings of mung bean (*Vigna radiata* L.). *Acta Physiol. Plant.* **2015**, *37*, 11.
(27) Vannini, C.; Domingo, G.; Onelli, E.; De Mattia, F.; Bruni, I.; Marsoni, M.; Bracale, M. Phytotoxic and genotoxic effects of silver nanoparticles exposure on germinating wheat seedlings. *J. Plant Physiol.* **2014**, *171*, 1142−1148.
(28) U.S. Research Nanomaterials, Inc. The Advanced Nanomaterials Provider. Copper (Cu) Nanopowder/Nanoparticles (Cu, 99.9%, 40 nm, metal basis), http://www.us-nano.com/inc/sdetail/162 (accessed on March 28, 2017).
(29) Hansch, R.; Mendel, R. R. Physiological functions of mineral micronutrients (Cu, Zn, Mn, Fe, Ni, Mo, B, Cl). *Curr. Opin. Plant Biol.* **2009**, *12*, 259−266.
(30) Zafar, H.; Ali, A.; Zia, M. CuO nanoparticles inhibited root growth from *Brassica nigra* seedlings but induced root from stem and leaf explants. *Appl. Biochem. Biotechnol.* **2017**, *181*, 365−378.
(31) Sarret, G.; Willems, G.; Isaure, M. P.; Marcus, M. A.; Fakra, S. C.; Frerot, H.; Pairis, S.; Geoffroy, N.; Manceau, A.; Saumitou-Laprade, P. Zinc distribution and speciation in *Arabidopsis halleri* x *Arabidopsis lyrata* progenies presenting various zinc accumulation capacities. *New Phytol.* **2009**, *184*, 581−595.
(32) Ravel, B.; Newville, M. ATHENA, ARTEMIS, HEPHAESTUS: data analysis for X-ray absorption spectroscopy using IFEFFIT. *J. Synchrotron Radiat.* **2005**, *12*, 537−541.
(33) Carvalho, H. W. P.; Hammer, P.; Pulcinelli, S. H.; Santilli, C. V.; Molina, E. F. Improvement of the photocatalytic activity of magnetite by Mn-incorporation. *Mater. Sci. Eng., B* **2014**, *181*, 64−69.
(34) Isani, G.; Falcioni, M. L.; Barucca, G.; Sekar, D.; Andreani, G.; Carpene, E.; Falcioni, G. Comparative toxicity of CuO nanoparticles and $CuSO_4$ in rainbow trout. *Ecotoxicol. Environ. Saf.* **2013**, *97*, 40−46.
(35) Carvalho, H. W. P.; Rocha, M. V. J.; Hammer, P.; Ramalho, T. C. TiO_2-Cu photocatalysts: a study on the long- and short-range chemical environment of the dopant. *J. Mater. Sci.* **2013**, *48*, 3904−3912.
(36) Pahlsson, A. M. B. Toxicity of heavy-metals (Zn, Cu, Cd, Pb) to vascular plants - a literature-review. *Water, Air, Soil Pollut.* **1989**, *47*, 287−319.
(37) Wojtyla, L.; Lechowska, K.; Kubala, S.; Garnczarska, M. Different modes of hydrogen peroxide action during seed germination. *Front. Plant Sci.* **2016**, *7*, 16.
(38) Shaw, A. K.; Hossain, Z. Impact of nano-CuO stress on rice (*Oryza sativa* L.) seedlings. *Chemosphere* **2013**, *93*, 906−915.
(39) Trujillo-Reyes, J.; Majumdar, S.; Botez, C. E.; Peralta-Videa, J. R.; Gardea-Torresdey, J. L. Exposure studies of core-shell Fe/Fe_3O_4 and Cu/CuO NPs to lettuce (*Lactuca sativa*) plants: are they a potential physiological and nutritional hazard? *J. Hazard. Mater.* **2014**, *267*, 255−263.
(40) Ajiboye, B.; Cakmak, I.; Paterson, D.; de Jonge, M. D.; Howard, D. L.; Stacey, S. P.; Torun, A. A.; Aydin, N.; McLaughlin, M. J. X-ray fluorescence microscopy of zinc localization in wheat grains biofortified through foliar zinc applications at different growth stages under field conditions. *Plant Soil* **2015**, *392*, 357−370.
(41) Kyriacou, B.; Moore, K. L.; Paterson, D.; de Jonge, M. D.; Howard, D. L.; Stangoulis, J.; Tester, M.; Lombi, E.; Johnson, A. A. T. Localization of iron in rice grain using synchrotron X-ray fluorescence microscopy and high resolution secondary ion mass spectrometry. *J. Cereal Sci.* **2014**, *59*, 173−180.
(42) Hernandez-Viezcas, J. A.; Castillo-Michel, H.; Andrews, J. C.; Cotte, M.; Rico, C.; Peralta-Videa, J. R.; Ge, Y.; Priester, J. H.; Holden, P. A.; Gardea-Torresdey, J. L. *In situ* synchrotron X-ray fluorescence mapping and speciation of CeO_2 and ZnO nanoparticles in soil cultivated soybean (*Glycine max*). *ACS Nano* **2013**, *7*, 1415−1423.
(43) Young, L.; Westcott, N.; Christensen, C.; Terry, J.; Lydiate, D.; Reaney, M. Inferring the geometry of fourth-period metallic elements in *Arabidopsis thaliana* seeds using synchrotron-based multi-angle X-ray fluorescence mapping. *Ann. Bot.* **2007**, *100*, 1357−1365.
(44) Vieira, C.; Paula Júnior, T. J.; Borém, A. Botânica. In *Feijão*, 2nd ed.; Universidade Federal de Viçosa: Viçosa, Brazil, 2006; 600 pages.
(45) Gunter, T.; Carvalho, H. W. P.; Doronkin, D. E.; Sheppard, T.; Glatzel, P.; Atkins, A. J.; Rudolph, J.; Jacob, C. R.; Casapu, M.; Grunwaldt, J. D. Structural snapshots of the SCR reaction mechanism on Cu-SSZ-13. *Chem. Commun.* **2015**, *51*, 9227−9230.
(46) Wang, Z. Y.; Xu, L. N.; Zhao, J.; Wang, X. K.; White, J. C.; Xing, B. S. CuO nanoparticle interaction with *Arabidopsis thaliana*: toxicity,

DOI: 10.1021/acs.jafc.7b03014
J. Agric. Food Chem. 2017, 65, 7874−7884

parent-progeny transfer, and gene expression. *Environ. Sci. Technol.* **2016**, *50*, 6008−6016.
(47) Yruela, I. Copper in plants: acquisition, transport and interactions. *Funct. Plant Biol.* **2009**, *36*, 409−430.
(48) Larue, C.; Laurette, J.; Herlin-Boime, N.; Khodja, H.; Fayard, B.; Flank, A. M.; Brisset, F.; Carriere, M. Accumulation, translocation and impact of TiO_2 nanoparticles in wheat (*Triticum aestivum* spp.): Influence of diameter and crystal phase. *Sci. Total Environ.* **2012**, *431*, 197−208.
(49) Chakraborty, D.; Damsgaard, C. D.; Silva, H.; Conradsen, C.; Olsen, J. L.; Carvalho, H. W. P.; Mutz, B.; Bligaard, T.; Hoffmann, M. J.; Grunwaldt, J. D.; Studt, F.; Chorkendorff, I. Bottom up design of a novel CuRu nanoparticulate catalyst for low temperature ammonia oxidation. *Angew. Chem., Int. Ed.* **2017**, *56*, 8711−8715.
(50) Lee, C. K.; Karunanithy, R. Effects of germination on the chemical-composition of *Glycine* and *Phaseolus* beans. *J. Sci. Food Agric.* **1990**, *51*, 437−445.
(51) Karmous, I.; Chaoui, A.; Jaouani, K.; Sheehan, D.; El Ferjani, E.; Scoccianti, V.; Crinelli, R. Role of the ubiquitin-proteasome pathway and some peptidases during seed germination and copper stress in bean cotyledons. *Plant Physiol. Biochem.* **2014**, *76*, 77−85.
(52) Sfaxi-Bousbih, A.; Chaoui, A.; El Ferjani, E. Unsuitable availability of nutrients in germinating bean embryos exposed to copper excess. *Biol. Trace Elem. Res.* **2010**, *135*, 295−303.

DOI: 10.1021/acs.jafc.7b03014
J. Agric. Food Chem. 2017, 65, 7874−7884